JOURNAL OF SYNCHROTRON RADIATION
ISSN 1600-5775

Computer-assisted area detector masking

Christopher J. Wright* and Xiao-Dong Zhou

Department of Chemical Engineering, University of South Carolina, Columbia, SC 29208, USA.
*Correspondence e-mail: cjwright4242@gmail.com

Received 6 August 2016
Accepted 4 January 2017

Edited by V. Favre-Nicolin, CEA and Université Joseph Fourier, France

Keywords: masking; area detector; Python.

Supporting information: this article has supporting information at journals.iucr.org/s

Area detectors have become the predominant type of detector for the rapid acquisition of X-ray diffraction, small-angle scattering and total scattering. These detectors record the scattering for a large area, giving each shot good statistical significance to the resulting scattered intensity $I(Q)$ pattern. However, many of these detectors have pixel level defects, which cause error in the resulting one-dimensional patterns. In this work, new software to automatically find and mask these dead pixels and other defects is presented. This algorithm is benchmarked with both ideal simulated and experimental datasets.

1. Introduction

In recent years, X-ray powder diffraction and X-ray total scattering techniques have been used to perform rapid *in situ* measurements at synchrotron radiation sources. This requires use of large two-dimensional area detectors with fast frame rates. Two-dimensional area detectors are especially important for atomic pair distribution function (PDF) analysis and other techniques which require large reciprocal space (Q-space) and good statistics at large Q (Chupas *et al.*, 2003). However, these detectors can have defects including dead/hot scintillators and pixels. In areas of low incident intensity these defects can cause data to become unreliable and thus unusable. In most azimuthal integration software, including *Fit2D* and *pyFAI*, these dead pixels are removed by masking the bad regions (Hammersley *et al.*, 1996; Kieffer & Karkoulis, 2013). These masks are usually produced manually or using an intensity threshold. In manual masking, each pixel is painstakingly examined for deviation from the proper value. While threshold masking is automatic, it has a tendency of removing large regions of data or missing the bad regions completely.

Voltolini *et al.* (2013) and Vamvakeros *et al.* (2015) have also addressed this masking issue in the context of X-ray diffraction tomography. Voltolini *et al.*'s work uses a combination of thresholding and mask dilation. However, it seems that large areas of pixels are replaced during the masking, even when some are not needing removal. The work by Vamvakeros *et al.* performs a two-dimensional integration before applying various statistical filters, including standard deviation trimmed mean. While the use of the two-dimensional integration is similar to the method presented here, the two-dimensional integration step, which usually requires a split pixel method, can cause unwanted covariances in the integrated data (Yang *et al.*, 2014).

We present a solution to this problem in the form of an automated mask writing program. This program will take

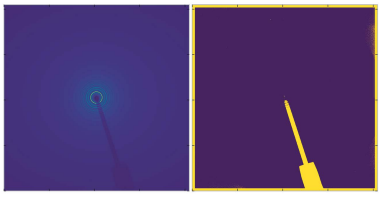

advantage of the inherent azimuthal symmetry of powder X-ray scattering to mask statistically significant outliers.

2. Methodology

In this method we have applied the automatic masking procedure to two-dimensional diffraction images which contain powder diffraction rings known as Debye–Scherrer rings (Billinge & Egami, 2012). The masking algorithm relies on measuring statistically significant outliers.

2.1. Algorithm design

To properly mask the detector the image must first be binned to its appropriate rings. To avoid issues of pixel size in Q space the binning is done in the detector radial space, with the resolution of each ring set to the diagonal of a single pixel. While this creates some issues with highly tilted detectors, most detector setups will be masked properly, as shown in the experimental benchmarking section. Once the bins are formed, the image is integrated twice, obtaining the mean value and standard deviation of each ring. Finally, each pixel that is α standard deviations away from the mean is masked. Note that the threshold α can be a function of distance from the point of incidence.

2.2. Test cases

To study the effectiveness of the masking we ran the algorithm against both simulated and experimental data. The simulated data test cases can be found in the supporting information.

Figs. 1 and 2 show experimental X-ray scattering recorded at beamline 11-ID-B at the Advanced Photon Source (APS) using a Perkin Elmer area detector for Pr_2NiO_4 at 50°C and a glass capillary, respectively. The wavelength was 0.143 Å^{-1}, the sample-to-detector distance was 25 cm and the images were recorded using *QXRD* software (Jennings, 2015). *pyFAI* was used to calibrate the detector, based on a CeO_2 standard. Each image was corrected for dark current and a beam polarization of 0.95 using *pyFAI*. Masks were computed for each image after the polarization correction. The Pr_2NiO_4 and glass images were acquired by summing 250 0.2 s exposures and 20 5 s exposures, respectively. Both masks were made with a threshold of two times the standard deviation. The integrations were performed using *pyFAI* with 1450 bins.

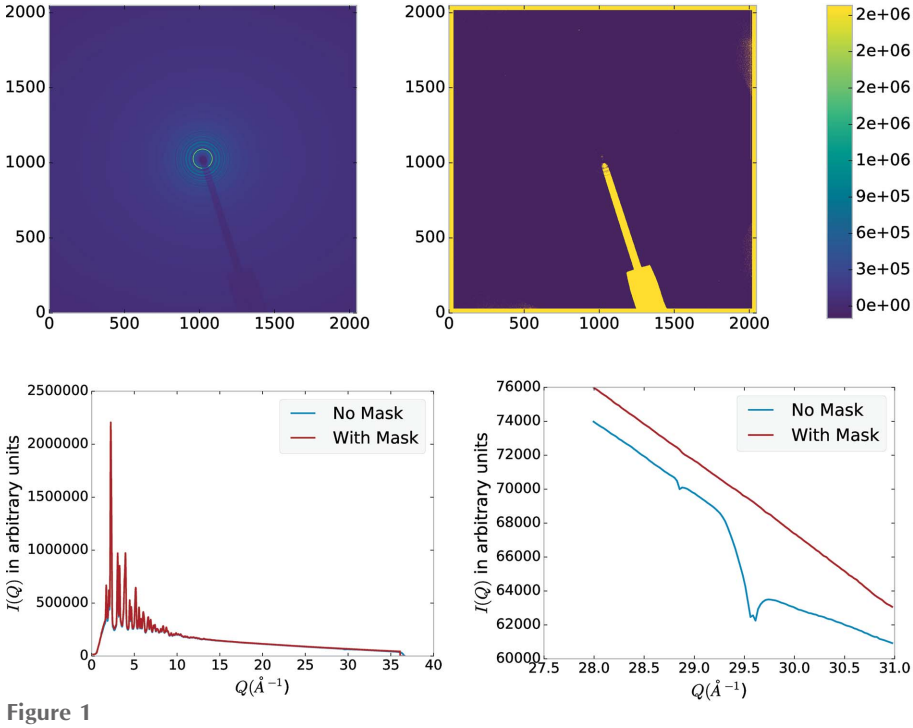

Figure 1
Masked experimental scattering from Pr_2NiO_4. Clockwise from the top left: raw image, resulting mask, integrated intensity with and without a mask from 28 to 31 Å^{-1}, full integrated intensity with and without a mask.

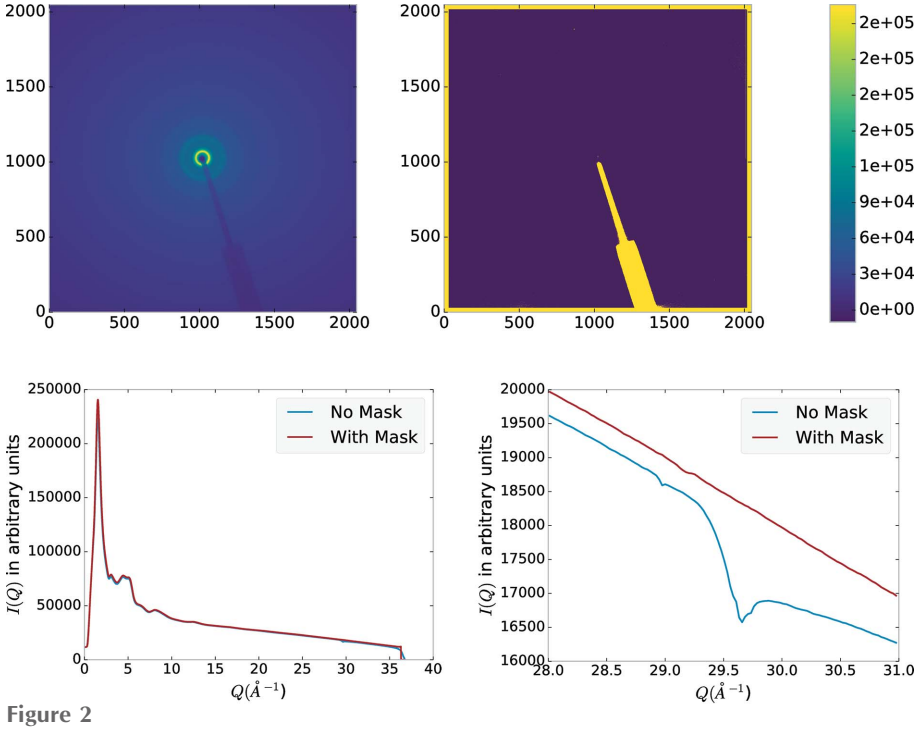

Figure 2
Masked experimental scattering from a glass capillary. Clockwise from the top left: raw image, resulting mask, integrated intensity with and without a mask from 28 to 31 Å^{-1}, full integrated intensity with and without a mask.

As previously shown with the simulated data, the beamstop holder is masked to very low Q values and the dead/hot pixels are properly removed. Unlike the simulated data, the experimental data also have streaks of dead pixels, which have also been properly removed. Proper data pre-processing, including dark current and polarization corrections, were found to be extremely important as these corrections helped to reduce the standard deviation of each ring, allowing for more bad pixels to be caught. Each dataset shows the removal of the 'high-Q kink' *via* masking. While the exact origin of the 'kink' is unknown, it may be due to a combination of the shadow from the beamstop holder and the edge defects in the detector. It is also important to note that the low-scattering glass-based mask captures more of the low-Q beamstop while there are missing rings in the medium-scattering Pr_2NiO_4 mask. This may be due to a combination of the sharpness of the Pr_2NiO_4 peaks and the detector tilt. Since the masking algorithm is not able to account for the detector tilt it can put pixels from two close, but distinct, rings in the same bin. This binning issue causes a higher standard deviation, since two proximal pixels could have very different values if one is on the Bragg peak and the other is not, allowing the beamstop pixels to slip under the threshold. This effect is less of a problem with the glass sample, where the changes in the intensity are more gradual, thus the error of putting two pixels in the same bin is smaller. This could potentially be remedied by using Q resolution binning which is corrected for detector tilt.

3. Conclusion

Overall, this work is a significant advancement in data processing for two-dimensional area detectors developing a robust and simple algorithm for masking. These advancements were tested against a series of both computationally and experimentally derived datasets. Most importantly, the masking and integration of the experimental datasets showed that proper masking can result in the removal of the high-Q 'kink' which had previously limited the extent of X-ray scattering which could be used for PDF analysis. Future work in this area may include the development of a tilt-corrected Q binning algorithm and examining different mathematical categorization of outliers. This work will not only help in advancing the most demanded *in situ* and high-throughput powder diffraction measurements but also provide reliable data from samples in complex environments.

This software is currently available on GitHub in the XPD workflow repository: https://github.com/CJ-Wright/xpd_workflow. This software will also be added to the more general scikit-beam repository in the near future: https://github.com/scikit-beam/scikit-beam.

Acknowledgements

The authors would like to thank the APS 11-ID-B team for helping with the data collection, the NSLS-II DAMA group for help with the software design, Dr Sanjit Ghose for his insights and thorough edits, James McClintock for working on the second iteration of this software, and Emir Dogdibegovic for providing the experimental sample. This material is based upon work supported under the National Science Foundation IGERT Grant No. 1250052 and USC Presidential Fellows Program.

References

Billinge, S. J. L. & Egami, T. (2012). *Underneath the Bragg Peaks: Structural Analysis of Complex Materials*, 2nd ed. Amsterdam: Elsevier.
Chupas, P. J., Qiu, X., Hanson, J. C., Lee, P. L., Grey, C. P. & Billinge, S. J. L. (2003). *J. Appl. Cryst.* **36**, 1342–1347.
Hammersley, A. P., Svensson, S. O., Hanfland, M., Fitch, A. N. & Hausermann, D. (1996). *High. Press. Res.* **14**, 235–248.
Jennings, G. (2015). *QXRD – Readout Software for Flat Panel X-ray Detectors*, http://qxrd.sourceforge.net/.
Kieffer, J. & Karkoulis, D. (2013). *J. Phys. Conf. Ser.* **425**, 202012.
Vamvakeros, A., Jacques, S. D. M., Di Michiel, M., Middelkoop, V., Egan, C. K., Cernik, R. J. & Beale, A. M. (2015). *J. Appl. Cryst.* **48**, 1943–1955.
Voltolini, M., Dalconi, M. C., Artioli, G., Parisatto, M., Valentini, L., Russo, V., Bonnin, A. & Tucoulou, R. (2013). *J. Appl. Cryst.* **46**, 142–152.
Yang, X., Juhás, P. & Billinge, S. J. L. (2014). *J. Appl. Cryst.* **47**, 1273–1283.